

Dynamics, Control, and Trajectory Tracking of Spacecraft Manipulators with Thrusters and Momentum Exchange Devices

Andrea Antonello*

University of Padova, Padova, 35131, Italy

Alfredo Valverde[†] and Panagiotis Tsiotras[‡]

Georgia Institute of Technology, Atlanta, Georgia 30332-0150, USA

The space sector is currently undergoing a push from industry, several governments, and academia to enable routine satellite servicing in orbit. Among the many challenges, the complex dynamic interactions between the satellite base and the robotic arm are of primary concern. While some missions may rely on the grappling of the host satellite, which would simplify servicing by virtue of fixing the relative kinematics between the two satellites, future space missions may also require single point-of-contact between two satellites. Thus, precise end-effector control of the maneuvering satellite and its base is required. While effective control tools exist in the fields of spacecraft pose control and robotics, simple methods to combine them lack in the space robotic servicing literature, which often requires complex derivations, and can be subject to constraints – as is the case with a fixed center of mass, or a zero angular momentum system. In this paper, we combine the well-known recursive Newton-Euler approach with appropriate spacecraft control algorithms to perform coordinated control of a spacecraft manipulator system. We discuss the interface between the two models (the base and the manipulator), and incorporate several realistic actuation models including thrusters and momentum exchange devices. In addition, we propose a novel actuation approach through a cluster of four Variable Speed Control Moment Gyroscopes (VSCMGs). The system is simulated and the proposed controllers implemented and tested according to the different actuation modes of the spacecraft. The simulation results are discussed and the performance during each scenario is analyzed.

Nomenclature

\otimes = Unit quaternion product operator

\mathcal{F} = Inertial frame of reference

*Postdoctoral Research Associate, Department of Information Engineering, Email: andrea.antonello.it@gmail.com.

[†]Ph.D. Candidate, School of Aerospace Engineering, Email: avalverde3@gatech.edu, AIAA Student Member.

[‡]Dean's Professor, School of Aerospace Engineering, Email: tsiotras@gatech.edu, AIAA Fellow.

\mathcal{B}	=	Satellite-body frame of reference
\mathcal{G}	=	Gimbal mount frame of reference
\mathcal{W}	=	Wheel frame of reference
$\{C, i\}$	=	Frame of reference with origin at the center of mass of body i , with axes aligned with frame i
R_x^y	=	Rotation matrix transforming coordinates from frame x to frame y
P_C^x	=	Position of point C , expressed in frame x
$P_{x/y}^z$	=	Position of the origin of frame x with respect to frame y , in frame z coordinates
$v_{x/y}^z, \omega_{x/y}^z$	=	Linear and angular velocity of frame x with respect to frame y , in frame z coordinates
$v_{x/y}, \omega_{x/y}$	=	Linear and angular velocity of frame x with respect to frame y , in frame x coordinates
$\dot{v}_{\{C,x\}/y}^z$	=	Acceleration of point C – fixed in frame x – with respect to frame y , in frame z coordinates
$h_{x/O}^y$	=	Angular momentum of body x , computed about point O and expressed in frame y coordinates
$q_{x/y}$	=	Unit quaternion from frame y to frame x
\mathbb{H}	=	Set of unit quaternions
$\dot{\gamma}$	=	Gimbal rate, [rad/s]
Ω	=	Wheel speed, [rad/s]
θ	=	Manipulator joint variable, [rad]
$M(\theta)$	=	Manipulator inertia matrix
$C(\theta, \dot{\theta})$	=	Manipulator Coriolis and centrifugal torques
$G(\theta)$	=	Manipulator gravitational torques
$J(\theta)$	=	Manipulator Jacobian matrix
τ_{arm}	=	Manipulator joint torques, [N/m]
τ_{wh}	=	VSCMGs torques, [N/m]
$I_{i/O}^x$	=	Inertia tensor of body i , computed about point O , expressed with respect to the x -frame
I_i^C	=	Inertia tensor of body i , computed and expressed in frame $\{C, i\}$ attached to the center of mass
$\mathbb{1}_N$	=	Identity matrix of size $N \times N$
$\mathbb{0}_N$	=	Null matrix of size $N \times N$
F_i^j, T_i^j	=	Force, torque acting on the center of mass of body i , in frame $\{j\}$ coordinates, [N] and [N/m]
F_i, T_i	=	Force, torque acting on the center of mass of body i , in frame $\{i\}$ coordinates, [N] and [N/m]
f_i^j, t_i^j	=	Force, torque exerted by link $i - 1$ on link i , in frame $\{j\}$ coordinates, [N] and [N/m]
f_i, t_i	=	Force, torque exerted by link $i - 1$ on link i , in frame $\{i\}$ coordinates, [N] and [N/m]
$f_{\text{thr}}^j, t_{\text{thr}}^j$	=	Force and moment exerted by the thrusters, in frame $\{j\}$ coordinates, [N] and [N/m]
σ	=	Vector of scalar thruster forces, [N]

I. Introduction

The theoretical interest to use robotic manipulators in space has flourished since the early 70's [1] and has evolved into a thoroughly studied field. JPL landed Viking I on Mars in 1976, claiming the race to the first use of a robotic arm outside of planet Earth. The first satellite-mounted robotic arm would come almost 20 years later, in 1998, when the ETS-VII [2] became the first experimental robotic arm to demonstrate grappling of another resident space object.

The main difficulty of performing robotic automated operations in orbit arises from the coupling between the movement of the arm and the satellite base. The literature thus far has mainly focused on generalizing the dynamics [3–5], which can be derived using different approaches. However, with increases in computational power, strides have been made in the development of different control strategies, including numerical algorithms from optimal and stochastic control [6–9]. Modern control algorithms also aim at minimizing the use of expendables, such as fuel and wear of the reaction wheels.

The push for robotic manipulation in space is led by a mixture of commercial and governmental stakeholders. For example, the ISS robotic arm, CANADARM, was a successful collaboration between Canadian industry and NASA [10]. Recently, the Robotic Servicing of Geosynchronous Satellites (RSGS) program by DARPA, aims at bridging the gap between technology development and deployment. The mission will capture, reposition, repair, and upgrade GEO satellites. NASA's RESTORE-L mission goal is to demonstrate autonomous rendezvous, docking, and servicing of orbiting spacecraft, with the ultimate objective of kickstarting the commercial space servicing industry. Both RSGS and RESTORE-L will utilize robotic arms to perform their respective missions.

The existing approaches when dealing with the arm-satellite coupling dynamics can be divided in two categories: internal control and coordinated control. The first approach [11–13] considers the motion of the free-floating platform — one in which the satellite base is not actively controlled — in the trajectory planning phase, and corrects the joint motions in order to compensate *a priori* for the motion of the base. This technique allows saving resources but requires a significantly more complicated control strategy, which is highly dependent on the robotic arm configuration [14].

In the second method, reaction control systems maintain a desired attitude and/or position of the base, depending on the types of actuators available, by counteracting the reaction torques and forces generated by the joints' movements. This configuration is referred to as a free-flying spacecraft [15]. This approach allows decoupling the planning of the joint trajectories from the motion of the base, and is useful when a particular base attitude is required (for example due to constraints imposed by communication, solar pointing, or payload, among others). On the other hand, a free-flying configuration requires expenditure of valuable resources, such as fuel or electrical power.

Several previous works in coordinated arm-satellite control are worth mentioning. Papadopoulos and Dubowsky [16] proposed a control method that extends the well known fixed-base Computed Torque Controller to the realm of satellite-mounted robotic manipulators. The authors did this by extending the state, and computing the appropriate generalized forces as a function of the base forces and torques, as well as the joint torques, to invert their relationship.

This inversion yields the forces and torques to be applied at the base, as well as the joint torques. Work by Carignan [17] outlines an intuitive and flexible development of the equations of motion, along with a control strategy to keep the satellite base stabilized, while the manipulator performs a given task. His work, however, pays no particular attention to the task performed by the end-effector. Jayakody et al [8] proposed a coordinated control method that is robust with respect to the mass properties of the system, and with respect to external disturbances. However, the algorithm does not provide an appropriate path planning strategy, and thus, inertial maneuvers cannot be achieved without manual *a priori* computations.

The purpose of this paper is twofold. First, we aim to develop a faithful simulator of a complex multibody system such as the free-floating and free-flying satellite with one or more manipulators mounted on it. In particular, the model is generalizable to any type of serial multibody system attached to the platform, and allows modeling any combination of the most common types of satellite-borne actuators, such as thrusters, reaction wheels and (variable speed) control moment gyroscopes. The validity of the model is assessed via checking the conservation of both linear and angular momentum, and by assessing the movement of the system's center of mass for a variety of different maneuvers, both in free floating and free flying modes.

The second goal of this work is to incorporate a control framework that can simultaneously deliver satisfactory performance for satellite-base stabilization and accurate end-effector pose tracking of a time-dependent trajectory. This is achieved by modeling the coupled dynamics with a modified version of the iterative Newton-Euler routine that accounts for the interaction between the satellite base and the manipulator, a feedback-linearization (through a Computed Torque Controller) control strategy for the arm, and a quaternion error feedback law for stabilization of the satellite base.

The approach allows for control of the satellite base using the VSCMGs in one of their three modes for attitude control (VSCMGs, CMG or RW), in combination with thrusters to perform station-keeping. This is the first work in which a complete solution for the multi-body dynamics problem with a VSCMGs actuated arm-satellite platform is provided. In addition, this is the first instance in which all possible combinations of actuators (thrusters, RW, MW, CMG, VSCMG) are considered in a unified framework to enable end-effector trajectory tracking for a space robotic manipulator.

The paper is structured as follows: in Section II, we introduce the satellite dynamics without any manipulator attached. Next, in Section III, we present the analysis of the manipulator alone, based on the recursive Newton-Euler algorithm. In Section IV, we merge the arm and satellite dynamics, obtaining a complete, recursive algorithm for the simulations of the coupled satellite-arm(s) system. In Section V, we incorporate a complete attitude control system by adding a cluster of Variable Speed Control Moment Gyroscopes (VSCMGs) and a set of fixed thrusters on the satellite. Section VI is dedicated to the development of the control laws for stabilization of the satellite base and pose tracking of the end-effector. Finally, in Section VII we present some simulations and characterize the performance of the proposed controller.

Notation Preliminaries

We define $\omega_{x/y}^z$ as the angular velocity of the frame x with respect to frame y , expressed in z -frame coordinates, and $v_{x/y}^z$ as the linear velocity of frame x with respect to frame y , and expressed in z -frame coordinates. In order to simplify the notation, the z superscript will be dropped when frame z is coincident with frame x . The matrix R_x^y will denote the rotation matrix that transforms coordinates from frame x to frame y .

The operator $[\cdot]^d$ is a square diagonal matrix defined such as, for a vector $x \in \mathbb{R}^{m \times 1}$,

$$[x]^d = \begin{bmatrix} x_1 & \dots & 0 \\ \vdots & \ddots & \vdots \\ 0 & \dots & x_m \end{bmatrix} \in \mathbb{R}^{m \times m}. \quad (1)$$

Calligraphic symbols will denote reference frames. Specifically, \mathcal{F} will denote the inertial reference frame, \mathcal{B} will denote the satellite body frame, $\{C, \mathcal{B}\}$ will denote the satellite body's center of mass frame and $\{i\}$ will denote the frame attached to link i of the robotic manipulator, whose center is defined by the Denavit-Hartenberg convention [18], which henceforth will be dropped for ease of notation. Frame $\{i = 0\}$ will indicate the manipulator base frame, fixed with respect to the satellite body.

II. Satellite Model

In this section, we present the general equations of a free-flying rigid body subject to internal and external actuation. This model will be further specialized to take into account the effect of a robotic arm attached to the main body. We approach this multibody problem by first decoupling the arm and the satellite dynamics. The mutual effects will be treated as external interactions between the two, and will be detailed in Section IV.

A. Dynamics

The linear and rotational dynamics of a rigid body can be described as follows

$$F_B^{\mathcal{F}} = m_B \dot{v}_{\{C, \mathcal{B}\}/\mathcal{F}}^{\mathcal{F}}, \quad (2)$$

$$T_B = I_B^C \dot{\omega}_{\mathcal{B}/\mathcal{F}} + \omega_{\mathcal{B}/\mathcal{F}} \times I_B^C \omega_{\mathcal{B}/\mathcal{F}}, \quad (3)$$

where $F_B^{\mathcal{F}}$ and T_B are the force and moment acting at the center of mass of the satellite body, respectively, expressed in the frame indicated by the superscript. Specifically, the term $\dot{v}_{\{C, \mathcal{B}\}/\mathcal{F}}^{\mathcal{F}}$ represents the acceleration of the satellite body's center of mass with respect to the inertial frame, expressed in inertial frame coordinates, whereas $\omega_{\mathcal{B}/\mathcal{F}}$ and $\dot{\omega}_{\mathcal{B}/\mathcal{F}}$ denote the angular velocity and acceleration of the satellite with respect to the inertial frame, expressed in body

coordinates. The satellite has mass m_B and inertia I_B^C , when expressed about the origin of the satellite's center of mass frame $\{C, \mathcal{B}\}$, with axes parallel to the \mathcal{B} frame.

If actuators are present, Eqs. (2) and (3) can be further specialized to

$$\sum f_{t,i}^{\mathcal{F}} = m_B \dot{v}_{\{C, \mathcal{B}\}/\mathcal{F}}^{\mathcal{F}}, \quad (4)$$

$$\sum P_{t,i}^{\mathcal{B}} \times f_{t,i}^{\mathcal{B}} = I_B^C \dot{\omega}_{\mathcal{B}/\mathcal{F}} + \omega_{\mathcal{B}/\mathcal{F}} \times I_B^C \omega_{\mathcal{B}/\mathcal{F}} + \dot{h}_{\text{med}}^{\mathcal{B}} + \omega_{\mathcal{B}/\mathcal{F}} \times h_{\text{med}}^{\mathcal{B}}, \quad (5)$$

where $f_{t,i}^{\mathcal{B}}$ represents the force generated by the i -th thruster, expressed in the body frame and mounted at the position $P_{t,i}^{\mathcal{B}}$ from the vehicle's center of mass. The terms \dot{h}_{med} and h_{med} account for the excess angular momentum of any momentum-exchange device mounted on the satellite. The general approach illustrated in Section V.B allows one to specialize the problem to any cluster of N (variable speed) control moment gyroscopes (VSCMG), momentum wheels (MW) or reaction wheels (RW).

B. Kinematics

The unit quaternion $q_{x/y}$ is used to describe the attitude of frame x with respect to frame y . We will often drop the subscripts when the relevant frames are obvious from the context, and use the simpler notation $q = (q_0, \bar{q})$ where $q \in \mathbb{H}$, with \mathbb{H} being the set of unit quaternions defined by $\mathbb{H} = \{q : q = q_0 + q_1i + q_2j + q_3k, q_0, q_1, q_2, q_3 \in \mathbb{R}, i^2 = j^2 = k^2 = -1, ijk = -1\}$, $q_0 \in \mathbb{R}$ is the scalar part of the quaternion, and $\bar{q} = [q_1, q_2, q_3]^T \in \mathbb{R}^3$ is the vector part of the quaternion. The unit quaternion can be constructed from the unit Euler axis \hat{n} and the Euler angle Φ as

$$q = \left(\cos \frac{\Phi}{2}, \hat{n} \sin \frac{\Phi}{2} \right). \quad (6)$$

The unit quaternion $q_{x/y}$ can be interpreted as a rotation of an angle Φ about the axis described by the unit vector \hat{n} . The kinematic differential equation describing the time evolution of the quaternion is given as [19]

$$\dot{q}_{x/y} = \frac{1}{2} q_{x/y} \otimes (0, \omega_{x/y}) = \frac{1}{2} (0, \omega_{x/y}^y) \otimes q_{x/y}, \quad (7)$$

where the operator \otimes denotes quaternion multiplication.

III. Manipulator Model

In this section we analyze the dynamics of the robotic arm as a standalone multibody system, with the aid of the recursive Newton-Euler method [20].

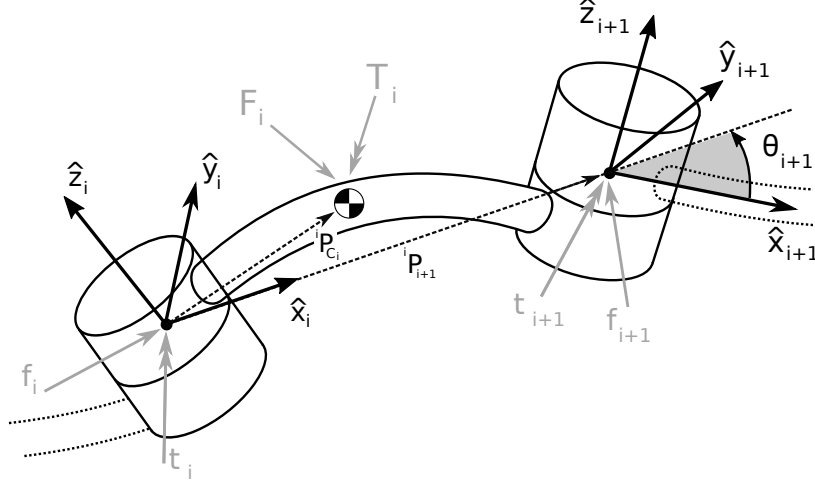


Fig. 1 Free body diagram of link i , with force balance

A. Dynamics: Newton-Euler Method

The Newton-Euler approach is based on the balance of all the forces and torques acting on a generic link of the manipulator. The solution of this problem is well suited for a recursive approach, thus making it our preferred choice for modeling the dynamics of the satellite-arm configuration. The method avoids complicated derivatives with respect to generalized coordinates, as it is common with Lagrangian-based approaches [19]. The recursive Newton-Euler algorithm can be implemented following the method introduced by Luh and Walker [20, 21]. The algorithm is composed of two parts: the *outward* iteration and the *inward* iteration. The first part consists of the calculation of the manipulator kinematics: computations are propagated from link 1 (the one closest to the base) to link N (the one closest to the end-effector) of the given chain; hence the name *outward*.

1. Outward Iteration

We first describe the notation used to develop the manipulator equations. Each link i has a frame $\{i\} \triangleq \{\hat{x}_i, \hat{y}_i, \hat{z}_i\}$ attached to it, according to the Denavit-Hartenberg convention [18] (refer to Fig. 1). The angle θ_{i+1} is the angle from link i to link $i+1$ computed at joint $i+1$ around the axis identified by the unit vector \hat{z}_{i+1} , the latter being expressed in frame $\{i+1\} \triangleq \{\hat{x}_{i+1}, \hat{y}_{i+1}, \hat{z}_{i+1}\}$. By further defining $\{C, i\}$ as the frame attached to link i , with the origin at the center of mass of link i and with the same axes orientation of frame $\{i\}$, the vector $P_{\{C, i\}/j}$ indicates the distance between the center of mass of link i and the origin of frame $\{j\}$, computed with respect to frame $\{j\}$ and expressed in frame $\{C, i\}$. Moreover, $v_{\{C, i\}/j}$ is the relative velocity of the center of mass of link i with respect to the origin of frame $\{j\}$ and expressed in frame $\{C, i\}$.

The kinematic propagation is obtained using the following equations

$$\omega_{i+1/\mathcal{F}} = R_i^{i+1} \omega_{i/\mathcal{F}} + \dot{\theta}_{i+1} \hat{z}_{i+1}, \quad (8)$$

$$\dot{\omega}_{i+1/\mathcal{F}} = R_i^{i+1} \dot{\omega}_{i/\mathcal{F}} + R_i^{i+1} \omega_{i/\mathcal{F}} \times \dot{\theta}_{i+1} \hat{z}_{i+1} + \ddot{\theta}_{i+1} \hat{z}_{i+1}, \quad (9)$$

$$\dot{v}_{\{C,i+1\}/\mathcal{F}} = \dot{v}_{i+1/\mathcal{F}} + \dot{\omega}_{i+1/\mathcal{F}} \times P_{\{C,i+1\}/i+1} + \omega_{i+1/\mathcal{F}} \times (\omega_{i+1/\mathcal{F}} \times P_{\{C,i+1\}/i+1}). \quad (10)$$

Applying Eqs. (2) and (3) we can calculate the inertial forces and torques applied on link $i+1$ using

$$F_{i+1} = m_{i+1} \dot{v}_{\{C,i+1\}/\mathcal{F}}, \quad (11)$$

$$T_{i+1} = I_{i+1}^C \dot{\omega}_{i+1/\mathcal{F}} + \omega_{i+1/\mathcal{F}} \times I_{i+1}^C \omega_{i+1/\mathcal{F}}, \quad (12)$$

where I_i^C is the inertia tensor of link i expressed in the frame $\{C, i\}$ attached to the link center of mass. This first set of equations is computed starting from $i = 0$ and arriving at $i = N - 1$.

2. Inward Iteration

In addition to the inertial force and torque computed in the outward iteration, each link experiences also the reactions exerted on it by the adjoining links. The free-body diagram of Fig. 1 yields the following equilibrium equations

$$F_i = f_i - R_{i+1}^i f_{i+1}, \quad (13)$$

$$T_i = t_i - R_{i+1}^i t_{i+1} - P_{\{C,i\}/i} \times f_i - (P_{i+1/i} - P_{\{C,i\}/i}) \times f_{i+1}^i, \quad (14)$$

where f_i is the force exerted by link $i - 1$ on link i , expressed in frame $\{i\}$, f_{i+1}^i is the force exerted by link i on link $i + 1$, expressed in frame $\{i\}$, t_i is the torque exerted by link $i - 1$ on link i , expressed in frame $\{i\}$, and $P_{i/j}$ indicates the distance between the origin of the frame attached to link i computed from the origin of the frame attached to link j and expressed in $\{i\}$ -frame coordinates. Equation (14) can be rearranged with the aid of Eq. (13) as

$$T_i = t_i - R_{i+1}^i t_{i+1} - P_{\{C,i\}/i} \times F_i - P_{i+1/i} \times R_{i+1}^i f_{i+1}. \quad (15)$$

Re-arranging Eqs. (13) and (15), we obtain the expressions needed to iteratively determine the reaction torque being applied at each joint. The equations are summarized as

$$f_i = F_i + R_{i+1}^i f_{i+1}, \quad (16)$$

$$t_i = T_i + R_{i+1}^i t_{i+1} + P_{\{C,i\}/i} \times F_i + P_{i+1/i}^i \times R_{i+1}^i f_{i+1}, \quad (17)$$

$$\tau_i = t_i^\top \hat{z}_i, \quad (18)$$

where τ_i is the scalar component of the joint torque t_i , projected along the \hat{z}_i axis, exerted by link $i - 1$ on link i . For $i = N$, the terms f_{N+1} and t_{N+1} appearing in Eqs. (13), (14) are defined as the external forces and torques acting on the end-effector, such as those generated by impacts or tool interactions, for example. We will denote these external forces and torques as $F_{\text{ext}} \triangleq [f_{N+1}, t_{N+1}]^\top$. Since the calculations are taken from the end-effector to the first link, the index count for the iterative solution will start at N and decrease to 1. Thus, this part of the algorithm is called the *inward* iteration.

Compactly, the Newton-Euler outward and inward routine can be summarized with the dynamic equation [22]

$$M(\theta)\ddot{\theta} + C(\theta, \dot{\theta}) + J(\theta)^\top F_{\text{ext}} + G(\theta) = \tau_{\text{arm}}, \quad (19)$$

where $M(\theta) \in \mathbb{R}^{N \times N}$ is the inertia matrix of the manipulator, $C(\theta, \dot{\theta}) \in \mathbb{R}^{N \times 1}$ contains the Coriolis and centrifugal torques, $J(\theta) \in \mathbb{R}^{N \times N}$ is the Jacobian mapping matrix, $F_{\text{ext}} \in \mathbb{R}^{N \times 1}$ is the vector of external forces and torques, $G(\theta) \in \mathbb{R}^{N \times 1}$ contains, if present, the gravitational torques, $\theta = [\theta_1, \dots, \theta_N]^\top \in \mathbb{R}^{N \times 1}$ is the joint variables vector and $\tau_{\text{arm}} = [\tau_1, \dots, \tau_N]^\top \in \mathbb{R}^{N \times 1}$ is the joint torque vector.

B. Free-flying Base and Boundary Conditions

For both inward and outward iterations, some starting conditions are needed. We first define the frame $\{0\} \triangleq \{\hat{x}_0, \hat{y}_0, \hat{z}_0\}$ as the frame attached to the first link of the manipulator, located at the joint that connects it with the satellite base. While this frame is fixed in the case of a fixed base manipulator, for a manipulator mounted on a free-flying body, frame $\{0\}$ is no longer inertial, and the quantities $\omega_{0/\mathcal{F}}, v_{0/\mathcal{F}}$ depend on the vehicle state as follows

$$\omega_{0/\mathcal{F}} = R_B^0 \omega_{B/\mathcal{F}} + \dot{\theta}_0 \hat{z}_0, \quad (20)$$

$$\dot{\omega}_{0/\mathcal{F}} = R_B^0 \dot{\omega}_{B/\mathcal{F}} + R_B^0 \omega_{B/\mathcal{F}} \times \dot{\theta}_0 \hat{z}_0 + \ddot{\theta}_0 \hat{z}_0, \quad (21)$$

$$\dot{v}_{0/\mathcal{F}} = R_B^0 [\dot{v}_{B/\mathcal{F}} + \dot{\omega}_{B/\mathcal{F}} \times P_{0/B}^B + \omega_{B/\mathcal{F}} \times (\omega_{B/\mathcal{F}} \times P_{0/B}^B)], \quad (22)$$

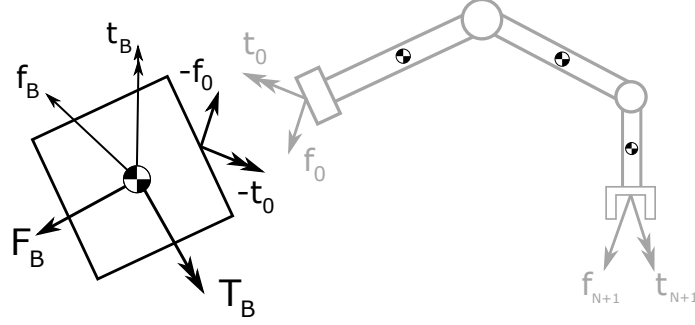


Fig. 2 Free body diagram of the satellite body, with indicated the manipulator reaction force f_0 and torque t_0 on the base platform

where $\omega_{\mathcal{B}/\mathcal{F}}$, $v_{\mathcal{B}/\mathcal{F}}$ are the angular and linear velocities of the body frame \mathcal{B} with respect to the inertial frame \mathcal{F} , expressed in \mathcal{B} body coordinates. Since the base frame of the manipulator $\{0\}$ is assumed to be rigidly attached to the satellite frame, \mathcal{B} , and since there is no relative motion between the two components it follows that $\dot{\theta}_0 = \ddot{\theta}_0 = 0$, Eqs. (20) and (21) simplify to

$$\omega_{0/\mathcal{F}} = R_{\mathcal{B}}^0 \omega_{\mathcal{B}/\mathcal{F}}, \quad (23)$$

$$\dot{\omega}_{0/\mathcal{F}} = R_{\mathcal{B}}^0 \dot{\omega}_{\mathcal{B}/\mathcal{F}}. \quad (24)$$

Therefore, at every iteration, after the initial conditions $\omega_{\mathcal{B}/\mathcal{F}}$, $\dot{\omega}_{\mathcal{B}/\mathcal{F}}$, $v_{\mathcal{B}/\mathcal{F}}$ and external forces and torques F_{ext} have been given, the *outward* and *inward* routines are run in sequence. These ultimately provide the reaction forces f_0 and t_0 acting on the manipulator base frame $\{0\}$ due to the arm's dynamics, and are obtained by propagating Eqs. (16) and (17) until $i = 0$. At the satellite body frame \mathcal{B} , the free-body diagram (Fig. 2) yields

$$f_{\mathcal{B}} = F_{\mathcal{B}} + R_0^{\mathcal{B}} f_0, \quad (25)$$

$$t_{\mathcal{B}} = T_{\mathcal{B}} + R_0^{\mathcal{B}} t_0 + P_{\{C, \mathcal{B}\}/\mathcal{B}} \times F_{\mathcal{B}} + P_{0/\mathcal{B}}^{\mathcal{B}} \times R_0^{\mathcal{B}} f_0, \quad (26)$$

where the vector $P_{\{C, \mathcal{B}\}/\mathcal{B}}$ is the offset between the frame with origin at the center of mass of body \mathcal{B} and the body frame itself, expressed in the \mathcal{B} frame.

IV. Model Integration

In summary, the equations of motion of a free-flying manipulator can be expressed as follows [23]

$$\begin{bmatrix} M & M_{mb} \\ M_{mb}^T & M_b \end{bmatrix} \begin{bmatrix} \ddot{\theta} \\ \ddot{x} \end{bmatrix} + \begin{bmatrix} C \\ C_b \end{bmatrix} + \begin{bmatrix} J^T \\ J_b^T \end{bmatrix} F_{\text{ext}} = \begin{bmatrix} \tau_{\text{arm}} \\ \mathcal{F}_B^{\mathcal{F}} \end{bmatrix}, \quad (27)$$

where M , C , J , and τ_{arm} are described as in Eq. (19), $M_b = \text{diag}([m\mathbb{1}^{3 \times 3}, J_B])$ is the inertia matrix of the satellite base, with $m = m_f + \sum_{k=1}^K m_{c,k}$, where m_f is the mass of the satellite frame without VSCMGs and $m_{c,k}$ is the mass of the k -th VSCMG. The inertia matrix J_B includes the satellite frame and the wheels, and its components are discussed in Section V.B. $M_{mb} \in \mathbb{R}^{N \times 6}$ is the coupling inertia matrix between the satellite base and the arm, $C_b \in \mathbb{R}^{6 \times 1}$ is the nonlinear Coriolis vector for the satellite base, $J_b \in \mathbb{R}^{6 \times 6}$ is the Jacobian matrix for the satellite base, $\mathcal{F}_B^{\mathcal{F}} = [f_B^{\mathcal{F}}, t_B^{\mathcal{F}}]^T \in \mathbb{R}^{6 \times 1}$ is the resultant of all the forces and torques applied by thrusters and wheels on the satellite, and $\ddot{x} = [\dot{v}_{B/\mathcal{F}}^{\mathcal{F}}, \dot{\omega}_{B/\mathcal{F}}^{\mathcal{F}}]^T \in \mathbb{R}^{6 \times 1}$ is the vector of generalized accelerations of the satellite base. Recalling that $-f_0$ and $-t_0$ are the force and torque applied on the satellite by the manipulator, and seen by the spacecraft as external contributions, it is possible to generalize the model to multiple manipulators. That is, the components $f_B^{\mathcal{F}}, t_B^{\mathcal{F}}$ of the force vector $\mathcal{F}_B^{\mathcal{F}}$ can be specialized, from Eqs. (25) and (26), as

$$f_B^{\mathcal{F}} = F_B^{\mathcal{F}} + \sum_p R_{0,p}^{\mathcal{F}} f_{0,p}, \quad (28)$$

$$t_B^{\mathcal{F}} = T_B^{\mathcal{F}} + P_{\{C,B\}/B}^{\mathcal{F}} \times F_B^{\mathcal{F}} + \sum_p R_{0,p}^{\mathcal{F}} t_{0,p} + P_{0,p/B}^{\mathcal{F}} \times R_{0,p}^{\mathcal{F}} f_{0,p}, \quad (29)$$

with $f_{0,p}, t_{0,p}$ being the force and torque exerted by the p -th manipulator on the satellite frame expressed in the p -th manipulator base frame $\{0, p\}$. Reasssuming these expressions into the forward dynamics [19, 23], one gets the comprehensive formulation for a manipulator mounted on a free-flying satellite*

$$\tilde{M}(P_{B/\mathcal{F}}^{\mathcal{F}}, q_{B/\mathcal{F}}, \theta) \begin{bmatrix} \ddot{\theta} \\ \dot{v}_{B/\mathcal{F}}^{\mathcal{F}} \\ \dot{\omega}_{B/\mathcal{F}}^{\mathcal{F}} \end{bmatrix} + \tilde{C}(P_{B/\mathcal{F}}^{\mathcal{F}}, q_{B/\mathcal{F}}, \dot{x}, \theta, \dot{\theta}) + \tilde{J}(P_{B/\mathcal{F}}^{\mathcal{F}}, q_{B/\mathcal{F}}, \theta)^T F_{\text{ext}} = \begin{bmatrix} \tau_{\text{arm}} \\ f_B^{\mathcal{F}} \\ t_B^{\mathcal{F}} \end{bmatrix}. \quad (30)$$

Due to the computational burden of obtaining the mass and Coriolis matrices analytically, one may resort to the numerical procedure described by Walker in [24] that yields the numerical values of $\tilde{M}(P_{B/\mathcal{F}}^{\mathcal{F}}, q_{B/\mathcal{F}}, \theta)$ and $\tilde{C}(P_{B/\mathcal{F}}^{\mathcal{F}}, q_{B/\mathcal{F}}, \dot{x}, \theta, \dot{\theta})$.

*The choice of expressing the parameters in the \mathcal{F} frame is arbitrary and they can be easily expressed in any other convenient frame through matrix frame multiplication.

With knowledge of each of the matrices, we can solve for the generalized acceleration vector as follows

$$\begin{bmatrix} \ddot{\theta} \\ \dot{v}_{\mathcal{B}/\mathcal{F}}^{\mathcal{F}} \\ \dot{\omega}_{\mathcal{B}/\mathcal{F}}^{\mathcal{F}} \end{bmatrix} = \tilde{M}(P_{\mathcal{B}/\mathcal{F}}^{\mathcal{F}}, q_{\mathcal{B}/\mathcal{F}}, \theta)^{-1} \begin{bmatrix} \tau_{\text{arm}} \\ f_{\mathcal{B}}^{\mathcal{F}} \\ t_{\mathcal{B}}^{\mathcal{F}} \end{bmatrix} - \tilde{C}(P_{\mathcal{B}/\mathcal{F}}^{\mathcal{F}}, q_{\mathcal{B}/\mathcal{F}}, \dot{x}, \theta, \dot{\theta}) - \tilde{J}(P_{\mathcal{B}/\mathcal{F}}^{\mathcal{F}}, q_{\mathcal{B}/\mathcal{F}}, \theta)^{\top} F_{\text{ext}}. \quad (31)$$

This generalized acceleration vector can then be integrated to obtain the new linear and angular velocities of the satellite base, $v_{\mathcal{B}/\mathcal{F}}$ and $\omega_{\mathcal{B}/\mathcal{F}}$, as well as the joint generalized velocities. The velocities are then used to propagate the satellite position $P_{\mathcal{B}/\mathcal{F}}^{\mathcal{F}}$ and the attitude quaternion $q_{\mathcal{B}/\mathcal{F}}$ from Eq. (7), as well as the new joint generalized coordinates.

V. Actuator Modeling

In this section, the main types of spacecraft actuators will be introduced and specialized to the problem of controlling a free-flying spacecraft. In particular, we will discuss the use of thrusters and momentum exchange devices.

A. Thrusters

The external forces and torques applied by a set of S thrusters are

$$f_{\text{thr}}^{\mathcal{B}} = \sum_{i=1}^S f_{\text{thr},i}^{\mathcal{B}}, \quad (32)$$

$$t_{\text{thr}}^{\mathcal{B}} = \sum_{i=1}^S P_{\text{thr},i/\{\mathcal{C},\mathcal{B}\}}^{\mathcal{B}} \times f_{\text{thr},i}^{\mathcal{B}}, \quad (33)$$

with $P_{\text{thr},i/\{\mathcal{C},\mathcal{B}\}}^{\mathcal{B}}$ being the relative position of thruster i with respect to origin of the satellite's center of mass frame, $\{\mathcal{C}, \mathcal{B}\}$, expressed in the \mathcal{B} frame. The effect of the thrusters on the dynamics can be modeled as [7, 25, 26]

$$\begin{bmatrix} f_{\text{thr}}^{\mathcal{B}} \\ t_{\text{thr}}^{\mathcal{B}} \end{bmatrix} = \begin{bmatrix} H_f \\ H_t \end{bmatrix} \sigma = H\sigma, \quad (34)$$

where $H_f, H_t \in \mathbb{R}^{3 \times S}$ are, respectively, the force and torque mapping matrices between the thrusters and the net force and torque on the mounting body, which depend on the placement of the thrusters with respect to the center of mass of the body. The vector $\sigma = (\sigma_1 \dots \sigma_i \dots \sigma_S)^{\top} \in \mathbb{R}^S$ contains the scalar thruster forces, that is $\sigma_i = \|f_{\text{thr},i}^{\mathcal{B}}\|$, exerted along the direction the thrusters are mounted, and which are lower- and upper-bounded as

$$\sigma_{\min} \leq \sigma_i \leq \sigma_{\max} \quad i = 1, 2, \dots, S. \quad (35)$$

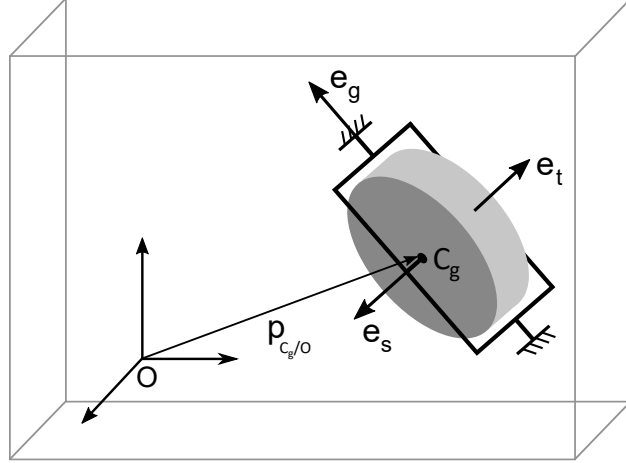


Fig. 3 VSCMGs notation

The lower and upper bounds $\sigma_{\min}, \sigma_{\max}$ are dictated by the thruster characteristics.

One way of determining the thruster firing allocation is by solving a linear program [27]. The problem then becomes one of finding σ such that

$$\sigma_{\text{opt}} = \underset{\sigma}{\operatorname{argmin}} \sum_{i=1}^S \sigma_i, \quad (36)$$

$$\text{subject to } \mathbf{H}_f \sigma = f_{\text{thr}}^B \quad (37)$$

$$\mathbf{H}_t \sigma = t_{\text{thr}}^B \quad (38)$$

$$\sigma_{\min} \leq \sigma_i \leq \sigma_{\max}, \quad i = 1, 2, \dots, S. \quad (39)$$

The optimum solution, if it exists, is then converted into the respective PWM duty cycle [6], as described in more detail in the simulation section.

B. Momentum Exchange Devices

Consider now a cluster of K single-gimbal VSCMGs. The vectors defining the gimbal frame \mathcal{G} for one VSCMG are pictured in Fig. 3 as follows:

- \hat{e}_s is the *spin* axis, along the spin axis of the wheel,
- \hat{e}_t is the *torque* axis that completes the gimbal frame $\mathcal{G} = \{\hat{e}_s, \hat{e}_t, \hat{e}_g\}$,
- \hat{e}_g is the *gimbal* axis, along the rotation axis of the gimbal.

The dynamic equations of motion for a satellite with a cluster of K VSCMGs have been developed in [28] and are presented here for convenience as

$$(\mathbf{A}_t[\dot{\gamma}]^d(\mathbf{I}_{cs} - \mathbf{I}_{ct})\mathbf{A}_s^T + \mathbf{A}_s[\dot{\gamma}]^d(\mathbf{I}_{cs} - \mathbf{I}_{ct})\mathbf{A}_t^T)\omega + \mathbf{J}\dot{\omega} + \mathbf{A}_g\mathbf{I}_{cg}\ddot{\gamma} + \mathbf{A}_t\mathbf{I}_{ws}[\Omega]^d\dot{\gamma} + \mathbf{A}_s\mathbf{I}_{ws}\dot{\Omega} + \omega \times (\mathbf{J}\omega + \mathbf{A}_g\mathbf{I}_{cg}\dot{\gamma} + \mathbf{A}_s\mathbf{I}_{ws}\Omega) = \mathbf{M}_{\text{ext}}, \quad (40)$$

where ω represents the angular velocity of the satellite with respect to the inertial frame, expressed in body coordinates, as defined in Eq. (2), in which subscripts have been dropped for simplicity. The matrix \mathbf{J} is the moment of inertia of the entire spacecraft, given by

$$\mathbf{J} = \mathbf{I}_B + \mathbf{A}_s\mathbf{I}_{cs}\mathbf{A}_s^T + \mathbf{A}_t\mathbf{I}_{ct}\mathbf{A}_t^T + \mathbf{A}_g\mathbf{I}_{cg}\mathbf{A}_g^T, \quad (41)$$

in which \mathbf{I}_B is the combined inertia matrix of the spacecraft frame inertia \mathbf{I}_B^C (see Eq. (3)), and of the distributed inertias of the wheels point masses. The matrices $\mathbf{I}_{c\star}$ are diagonal with elements the combination of the inertia values of the gimbal plus wheel structure, such that $\mathbf{I}_{c\star} = \mathbf{I}_{g\star} + \mathbf{I}_{w\star}$, with $\mathbf{I}_{g\star} = \text{diag}[\mathbf{I}_{g\star 1}, \dots, \mathbf{I}_{g\star K}]$ and $\mathbf{I}_{w\star} = \text{diag}[\mathbf{I}_{w\star 1}, \dots, \mathbf{I}_{w\star K}]$, where \star is s , t or g . The matrix $\mathbf{A}_\star = [e_{\star 1}, \dots, e_{\star K}] \in \mathbb{R}^{3 \times K}$ contains the spin, torque and gimbal unit vectors expressed with respect to the B frame and the column vectors $\gamma = (\gamma_1 \dots \gamma_K)^T \in \mathbb{R}^{K \times 1}$ and $\Omega = (\Omega_1 \dots \Omega_K)^T \in \mathbb{R}^{K \times 1}$ contain the gimbal angles and the spin rates of the VSCMGs, respectively. Two specialized cases of equation (40) can be highlighted. In the case where the VSCMGs are operated as conventional control moment gyroscopes (CMG), in which case $\dot{\Omega} = 0$, Eq. (40) becomes

$$(\mathbf{A}_t[\dot{\gamma}]^d\mathbf{I}_{cst}\mathbf{A}_s^T + \mathbf{A}_s[\dot{\gamma}]^d\mathbf{I}_{cst}\mathbf{A}_t^T)\omega + \mathbf{J}\dot{\omega} + \mathbf{A}_g\mathbf{I}_{cg}\ddot{\gamma} + \mathbf{A}_t\mathbf{I}_{ws}[\Omega]^d\dot{\gamma} + \omega \times (\mathbf{J}\omega + \mathbf{A}_g\mathbf{I}_{cg}\dot{\gamma} + \mathbf{A}_s\mathbf{I}_{ws}\Omega) = \mathbf{M}_{\text{ext}}. \quad (42)$$

When the VSCMGs are operated as reaction wheels (RW), in which case $\ddot{\gamma} = \dot{\gamma} = 0$, we have that

$$\mathbf{J}\dot{\omega} + \mathbf{A}_s\mathbf{I}_{ws}\dot{\Omega} + \omega \times (\mathbf{J}\omega + \mathbf{A}_s\mathbf{I}_{ws}\Omega) = \mathbf{M}_{\text{ext}}. \quad (43)$$

These three cases define the different VSCMG operational modes: VSCMGs, CMG or RW.

VI. Control Implementation

In our approach, we have decoupled the control of the manipulator and the control of the satellite base and we develop algorithms to control each one independently. The manipulator will be controlled using the Computed Torque Control (CTC) approach [29], while the satellite base will be controlled using a combination of thrusters and VSCMGs in one of their three operational modes: VSCMGs, CMG, or RWs. These control strategies are discussed next.

Manipulator Control: CTC

The dynamics of a manipulator arm with N joints, mounted on a satellite base, was introduced in Eq. (27)

$$M(\theta)\ddot{\theta} + C(\theta, \dot{\theta}) + J(\theta)^\top F_{\text{ext}} = \tau_{\text{arm}}. \quad (44)$$

Our objective is to track a reference trajectory $\xi_d(t) \in SE(3)$, where ξ_d is the desired end-effector pose. The trajectory $\xi_d(t)$ can be expressed in the joint space by using the inverse kinematics and inverse differential kinematics equations in [21], which yields the desired generalized coordinates and generalized speeds, respectively, as

$$\begin{aligned} \theta_d &= \mathcal{K}^{-1}(\xi_d), \\ \dot{\theta}_d &= J(\theta)^{-1} \dot{\xi}_d. \end{aligned} \quad (45)$$

Defining the tracking error of the desired trajectory, $e(t) \in \mathbb{R}^N$, as

$$e(t) \triangleq \theta_d(t) - \theta(t), \quad (46)$$

defining the control law

$$\tau_{\text{arm}} = M(K_p e + K_d \dot{e}) + M\ddot{\theta}_d + C, \quad (47)$$

and using the fact that $\ddot{\theta} = M^{-1}(\tau_{\text{arm}} - C)$, the closed loop error dynamics can be shown to evolve as

$$\ddot{e} + K_d \dot{e} + K_p e = 0. \quad (48)$$

The error dynamics thus represent an asymptotically stable linear system under the classical hypothesis of symmetric and positive definite gain matrices $K_p, K_d \in \mathbb{R}^{N \times N}$.

Attitude Control with Momentum Exchange Devices

Manipulating Eq. (40) by moving the terms containing the control parameters $\dot{\gamma}, \dot{\Omega}$ to the right-hand side, one obtains

$$\begin{aligned} J\dot{\omega} + \omega \times J\omega &= M_{\text{ext}} - (A_r[\dot{\gamma}]^d I_{\text{cst}} A_s^\top + A_s[\dot{\gamma}]^d I_{\text{cst}} A_r^\top) \omega - (A_g I_{\text{cg}} \dot{\gamma} + A_r I_{\text{ws}} [\dot{\Omega}]^d \dot{\gamma} + A_s I_{\text{ws}} \dot{\Omega}) \\ &\quad - \omega \times (A_g I_{\text{cg}} \dot{\gamma} + A_s I_{\text{ws}} \dot{\Omega}) \\ &= M_{\text{ext}} - \dot{J}\omega - \dot{h}_{\text{med}} - \omega \times h_{\text{med}} = M_{\text{ext}} + \tau_{\text{wh}}, \end{aligned} \quad (49)$$

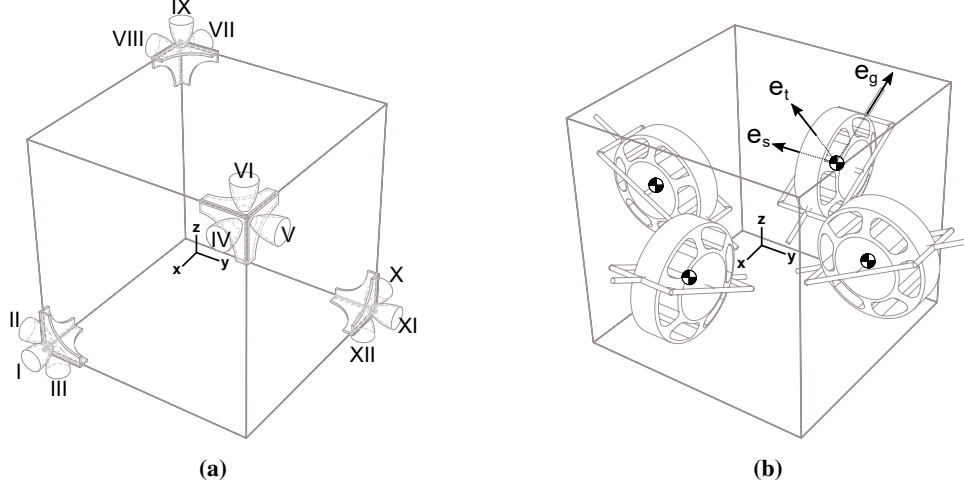


Fig. 4 Thrusters reaction control and VSCMGs configuration (satellite only)

where we have defined

$$\tau_{wh} \triangleq -\dot{J}\omega - \dot{h}_{med} - \omega \times h_{med}. \quad (50)$$

The right-hand side contains the control torque to be applied to the satellite by the actuation of the wheels, which is a function of the control inputs $\dot{\gamma}$ and $\dot{\Omega}$. In this work, we neglect the gimbal acceleration $\ddot{\gamma}$ since the dynamic contribution of $A_g I_{cg}$ is small compared to the later defined C and D matrices [30, 31].

Recalling that $[a]^d b = [b]^d a$, the product $\dot{J}\omega$ can be re-written as

$$\dot{J}\omega = (A_t I_{cst} [A_s^T \omega]^d + A_s I_{cst} [A_t^T \omega]^d) \dot{\gamma} \triangleq W \dot{\gamma}. \quad (51)$$

The exerted wheel torque then becomes

$$\begin{aligned} \tau_{wh} &= -W \dot{\gamma} - A_t I_{ws} [\Omega]^d \dot{\gamma} - A_s I_{ws} \dot{\Omega} - [\omega^\times] A_g I_{cg} \dot{\gamma} - [\omega^\times] A_s I_{ws} \Omega \\ &= - \begin{bmatrix} C & D \end{bmatrix} \begin{bmatrix} \dot{\gamma} \\ \dot{\Omega} \end{bmatrix} - \tau_{gy}, \end{aligned} \quad (52)$$

where the notation $[\omega^\times]$ denotes the skew-symmetric operator. Moreover, we define

$$\begin{aligned} C &\triangleq W + A_t I_{ws} [\Omega]^d + [\omega^\times] A_g I_{cg}, \\ D &\triangleq A_s I_{ws}, \\ \tau_{gy} &\triangleq [\omega^\times] A_s I_{ws} \Omega, \end{aligned} \quad (53)$$

with τ_{gy} being the gyroscopic torque. Finally, by making the dependencies explicit, τ_{wh} can be written as

$$\tau_{\text{wh}} = -\mathbf{G}(\omega, \gamma, \Omega) \begin{bmatrix} \dot{\gamma} \\ \dot{\Omega} \end{bmatrix} - \tau_{\text{gy}}(\omega, \gamma, \Omega). \quad (54)$$

The system can thus be expressed as

$$\mathbf{J}\dot{\omega} + \omega \times \mathbf{J}\omega = \mathbf{M}_{\text{ext}} + \tau_{\text{wh}} = \mathbf{M}_{\text{ext}} - \mathbf{G} \begin{bmatrix} \dot{\gamma} \\ \dot{\Omega} \end{bmatrix} - \tau_{\text{gy}}. \quad (55)$$

If we desire to apply a control τ_c using the VSCMGs, it suffices to equate τ_c to τ_{wh} to obtain

$$-\mathbf{G} \begin{bmatrix} \dot{\gamma} \\ \dot{\Omega} \end{bmatrix} - \tau_{\text{gy}} = \tau_c. \quad (56)$$

Solving for the control inputs $\dot{\gamma}$ and $\dot{\Omega}$ yields

$$\begin{bmatrix} \dot{\gamma} \\ \dot{\Omega} \end{bmatrix} = -\mathbf{G}^\dagger (\tau_c + \tau_{\text{gy}}), \quad (57)$$

where \mathbf{G}^\dagger is the weighted pseudoinverse [19]

$$\mathbf{G}^\dagger = \mathcal{W}\mathbf{G}^\top(\mathbf{G}\mathcal{W}\mathbf{G}^\top)^{-1}, \quad (58)$$

with \mathcal{W} defined as the weight diagonal matrix

$$\mathcal{W} \triangleq \begin{bmatrix} \alpha \mathbf{1}_K & \mathbf{0}_K \\ \mathbf{0}_K & \beta \mathbf{1}_K \end{bmatrix}, \quad (59)$$

where $\mathbf{1}_K$ identifies the $K \times K$ identity matrix and $\mathbf{0}_K$ is the $K \times K$ null matrix. The positive gains α and β define the operational mode of the VSCMG cluster: large values of α/β prioritize the CMG mode, while the opposite focuses the control on RW operation. In particular, it is possible to enforce a pure RW or CMG operation by setting $\alpha = 0$ or $\beta = 0$

respectively, with which we define

$$\mathcal{W}_{\text{RW}} = \begin{bmatrix} \mathbf{0}_K & \mathbf{0}_K \\ \mathbf{0}_K & \mathbf{1}_K \end{bmatrix}, \quad \mathcal{W}_{\text{CMG}} = \begin{bmatrix} \mathbf{1}_K & \mathbf{0}_K \\ \mathbf{0}_K & \mathbf{0}_K \end{bmatrix}. \quad (60)$$

Coordinated Attitude or Pose Control

Given the current actuator configuration (thrusters and VSCMGs), several possible control strategies exist for coordinated control of the satellite base. First, we explore the allocation of the commanded torque only via the VSCMGs. Next, we discuss the case where the attitude control is performed using the momentum exchange devices, as discussed in the previous section, while the position control (station-keeping) is performed using the satellite-mounted thrusters. The final strategy consists of controlling both the attitude and the position with thrusters only.

Momentum Exchange Devices

In the case when we desire to stabilize only the attitude of the base and the angular velocity with respect to some stationary desired reference, we can use the well-known quaternion error feedback law to control the base of the spacecraft

$$\tau_c = -K_1 \bar{q}_{B/D} - K_2 \omega_{B/D} - T_0^B, \quad (61)$$

where $\omega_{B/D} = \omega_{B/\mathcal{F}} - \omega_{D/\mathcal{F}}^B$ is the error between the actual and the desired angular velocities, denoted by $\omega_{B/\mathcal{F}}$ and $\omega_{D/\mathcal{F}}^B$ respectively, expressed in the body frame. The feedforward term $T_0^B = -R_0^B t_0 - P_{0/B}^B \times R_0^B f_0$ denotes the disturbance torque imparted on the spacecraft base due to the movement of the manipulator, as discussed in Eqs. (25) and (26). The gain matrices $K_1, K_2 \in \mathbb{R}^{3 \times 3}$ are positive definite and the quaternion error $q_{B/D} = (q_{0,B/D}, \bar{q}_{B/D}) \in \mathbb{H}$ is computed as [32–34]

$$q_{B/D} = q_{D/\mathcal{F}}^* \otimes q_{B/\mathcal{F}}, \quad (62)$$

with $q_{D/\mathcal{F}}, q_{B/\mathcal{F}} \in \mathbb{H}$ being the desired and actual attitude quaternion of the satellite base respectively, and with $q^* = (q_0, -\bar{q}) \in \mathbb{H}$ representing the quaternion conjugate. Setting $\tau_{\text{wh}} = \tau_c$, one obtains

$$-G \begin{bmatrix} \dot{\gamma} \\ \dot{\Omega} \end{bmatrix} - \tau_{\text{gy}} = -K_1 \bar{q}_{B/D} - K_2 \omega_{B/D} \implies \begin{bmatrix} \dot{\gamma} \\ \dot{\Omega} \end{bmatrix} = G^\dagger (K_1 \bar{q}_{B/D} + K_2 \omega_{B/D} - \tau_{\text{gy}}). \quad (63)$$

Mixed Momentum Exchange Devices and Thrusters Control

For the second control allocation case, the following error feedback laws are chosen

$$f_{\text{thr}}^{\mathcal{B}} = -K_{11}P_{\mathcal{B}/\mathcal{D}} - K_{12}v_{\mathcal{B}/\mathcal{D}} - F_0^{\mathcal{B}}, \quad (64)$$

$$\tau_c = -K_{21}\bar{q}_{\mathcal{B}/\mathcal{D}} - K_{22}\omega_{\mathcal{B}/\mathcal{D}} - T_0^{\mathcal{B}}, \quad (65)$$

where Eq. (65) is derived from the previous paragraph, and Eq. (64) contains the position and velocity errors of the satellite's base, namely $P_{\mathcal{B}/\mathcal{D}} = P_{\mathcal{B}/\mathcal{F}} - P_{\mathcal{D}/\mathcal{F}}^{\mathcal{B}}$ and $v_{\mathcal{B}/\mathcal{D}} = v_{\mathcal{B}/\mathcal{F}} - v_{\mathcal{D}/\mathcal{F}}^{\mathcal{B}}$, with $P_{\mathcal{D}/\mathcal{F}}^{\mathcal{B}}$, $v_{\mathcal{D}/\mathcal{F}}^{\mathcal{B}}$ being the desired position and velocity, respectively. In addition, the feedforward terms $F_0^{\mathcal{B}} = -R_0^{\mathcal{B}}f_0$ and $T_0^{\mathcal{B}}$ account for the disturbances induced by the dynamics of the manipulator. In the case of station-keeping, the desired velocity is set to zero, while the desired position is set to some initial constant reference. The gain matrices $K_{ij} \in \mathbb{R}^{3 \times 3}$ ($i, j = 1, 2$) are positive definite. The optimization algorithm of Eq. (36), subject to $H_f \sigma = f_{\text{thr}}^{\mathcal{B}}$ and $H_t \sigma = 0$ (since the torque contribution is provided solely by the momentum exchange devices), yields the solution to the firing allocation problem.

Full Thruster Control

In the case of full thruster control with no momentum exchange devices, the error feedback laws are as in Eq. (64) and (65)

$$f_{\text{thr}}^{\mathcal{B}} = -K_{11}P_{\mathcal{B}/\mathcal{D}} - K_{12}v_{\mathcal{B}/\mathcal{D}} - F_0^{\mathcal{B}}, \quad (66)$$

$$t_{\text{thr}}^{\mathcal{B}} = -K_{21}\bar{q}_{\mathcal{B}/\mathcal{D}} - K_{22}\omega_{\mathcal{B}/\mathcal{D}} - T_0^{\mathcal{B}}, \quad (67)$$

where the gain matrices $K_{ij} \in \mathbb{R}^{3 \times 3}$ ($i, j = 1, 2$) are positive definite. In this case, the thrusters perform both attitude and position control, and the optimization algorithm of Eq. (36) will be subject to $H_f \sigma = f_{\text{thr}}^{\mathcal{B}}$ and $H_t \sigma = t_{\text{thr}}^{\mathcal{B}}$.

VII. Numerical Simulations

In this section, we present the results from numerical simulations of a sample trajectory to test the validity of the proposed approach. The goal is for the manipulator end-effector to track a pre-defined pose along a given path, while maintaining the satellite base at a desired attitude (while is free to translate in the case of VSCMGs), and perform station-keeping with the aid of the on-board thrusters and/or the VSCMGs cluster. We use a standard four-wheel VSCMGs pyramid configuration, as depicted in Fig. 4 (b). Twelve jets are used in the numerical experiments below. Their geometric mounting on the satellite can be seen in Fig. 4 (a). We implemented a fully actuated thruster configuration such that it is always possible to generate a reaction force and torque along any direction [7].

The inertia parameters for the satellite, the wheels, the robotic manipulator and the thrusters are provided in Tables 1, 2 and 3. Several three-dimensional trajectories were given as target trajectories for the end-effector to track.

For the purpose of this work, we only present the results from a lemniscate trajectory, which is parametrized in Cartesian space as follows

$$\mathbf{x}(t) = \begin{cases} x = r[1 + \cos(\zeta t + \theta_{\text{in}})] + x_0, \\ y = r \sin(\zeta t + \theta_{\text{in}}) + y_0, \\ z = z_0. \end{cases}$$

Here, r represents the radius of the arc, ζ is the curve's angular velocity, θ_{in} is the initial offset angle and $P_{0/\mathcal{F}}^{\mathcal{F}} = [x_0, y_0, z_0]^T$ is the origin of the curve in inertial coordinates. The parameters are chosen as $r = 0.25$ m, $\theta_{\text{in}} = 0.1$ rad, $P_{0/\mathcal{F}}^{\mathcal{F}} = [1.25, 0.5, 2.25]^T$ m, $\zeta = 0.5$ rad/s. The starting joint variable vector is $\theta_0 = [0, \pi/6, -\pi/3, 0, 0, 0]^T$ rad and the initial position of the satellite body in inertial space is $P_{\mathcal{B}/\mathcal{F}}^{\mathcal{F}} = [0.5, 0.5, 0.5]^T$ m.

The satellite is controlled using any combination of actuators: none, wheels only, thrusters only or a combination of wheels and thrusters. Moreover, it is also possible to use the VSCMGs cluster in pure CMG or pure RW mode. Two different geometric trajectories are to be tracked using three different control approaches to demonstrate the differences in operation: uncontrolled, VSCMG-only control, and thrusters-only control. The pose of the end-effector can be commanded to track a desired attitude, either in Cartesian space or with respect to a frame attached to any of the links. In each of the examples analyzed, the desired pose of the end-effector is set to track a moving reference frame in inertial space, represented by the frame attached to link 4. The wheels are mounted at an angle of 54° with respect to the body \hat{z} -axis, with an initial gimbal angle $\gamma = 0_{4 \times 1}$ and a starting wheel idle speed of 2,500 rpm. As shown in Figs. 5 and 6, the tracking performance of the system without any control on the base lacks tracking accuracy. Fig. 7 shows the performance for the attitude-only tracking case, when the VSCMGs are switched on. It is clear that the residual movement of the center of mass is still substantial, on the order of ± 40 cm. This movement is drastically reduced when the thrusters are used (Fig. 9), allowing for accurate station-keeping. With the chosen PWM firing strategy, the errors in the satellite center of mass movement with respect to the starting position are below ± 1 cm. This performance is dependent on the bandwidth of the pulse-width controller and on the dead-zone and hysteresis characteristic of the *on-off* Schmitt trigger [35, 36]. Note that the time delay needed to switch the jets on and off and the hysteresis in the Schmitt trigger results in a limit cycle around the desired satellite pose [35].

The controlled motion of the satellite and the excellent tracking capabilities of the manipulator's end-effector are depicted in Figs. 8 and 10 for the VSCMGs and thrusters actuation, respectively. It should be noted that the use of VSCMGs allows only orientation control of the base, which can otherwise translate along all three axes. The use of thrusters allows the satellite base to remain completely stationary in inertial space. These 3D animations, obtained through a visual implementation of the multibody simulation tool, are shown for discrete timestamps of the maneuver, and allow to appreciate the vicinity between the commanded trajectory (solid blue line) and the actual

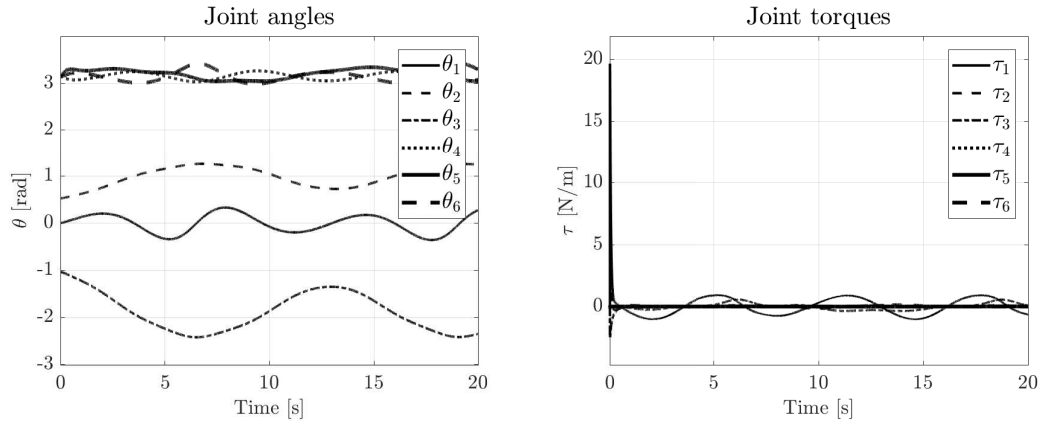
performance (solid grey line). Animations of the satellite/manipulator system performing these maneuvers can be found at <https://www.youtube.com/playlist?list=PLJbI5NA6udpGpEch4Ej6McjUsqDUNkBNq>.

VIII. Conclusions

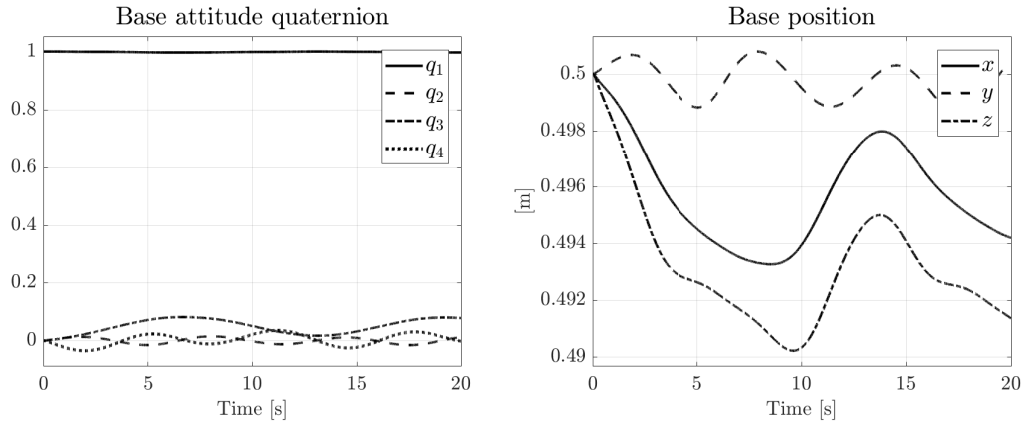
The problem of controlling a robotic arm mounted on a spacecraft has been studied in this paper. Different elements of the modeling and the control of such a system to perform precise pose-tracking of the end-effector are combined in an unified modeling framework. Traditional translational and rotational dynamics for the satellite base are combined with the recursive Newton-Euler algorithm for the dynamics of the manipulator. The interaction is addressed as an exchange of forces and torques at the manipulator base joint. The approach allows for control of the satellite base using the VSCMGs in one of their three modes for attitude control (VSCMGs, CMG or RW), in combination with thrusters to perform station-keeping. This is the first work in which end-effector pose tracking for a manipulator mounted on a satellite has been performed through the combined use of VSCMGs and thrusters. Also, this is the first work in the literature in which a complete solution for the multi-body dynamics problem for a VSCMGs actuated arm-satellite platform is provided and demonstrated.

The approach used consists of decoupling the satellite and the arm dynamics to stabilize the base, while the robotic arm performs a predetermined task. Typically, trajectory tracking of the end-effector and base stabilization have been treated in a decoupled manner. This paper aims to close the gap between the two approaches by providing a formulation that captures the coupling between the satellite base and the robotic arm to perform not only base stabilization (position and attitude), but also end-effector trajectory tracking of a desired path. Additionally, and as opposed to works in recursive dynamics previously proposed by Yoshida [37] and Carignan [17], we have proposed the incorporation of a tracking control scheme into the framework, as well as the modeling of realistic actuators. In particular, we use thrusters for the application of forces on the satellite base and Variable Speed Control Moment Gyros (VSCMGs) for attitude control, leading to a seamless integration with the recursive Newton-Euler approach that allows for accurate end-effector pose control.

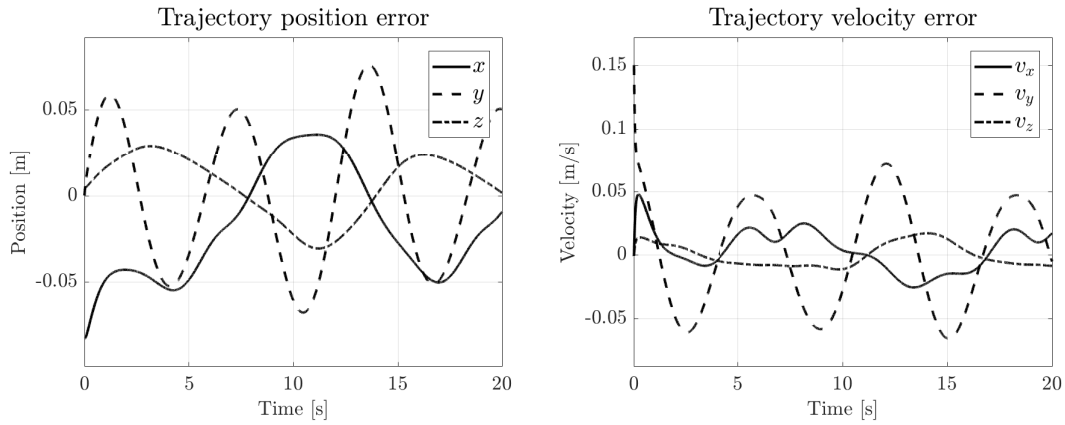
Several possible venues for research are left open for further investigation. The study of feedback control during the contact phase is essential for maintaining stability of the overall system. Studying the optimal switching from the proposed control framework to, say, an impedance controller for secure contact remains an active topic of research.



(a) Manipulator joint angles and torques

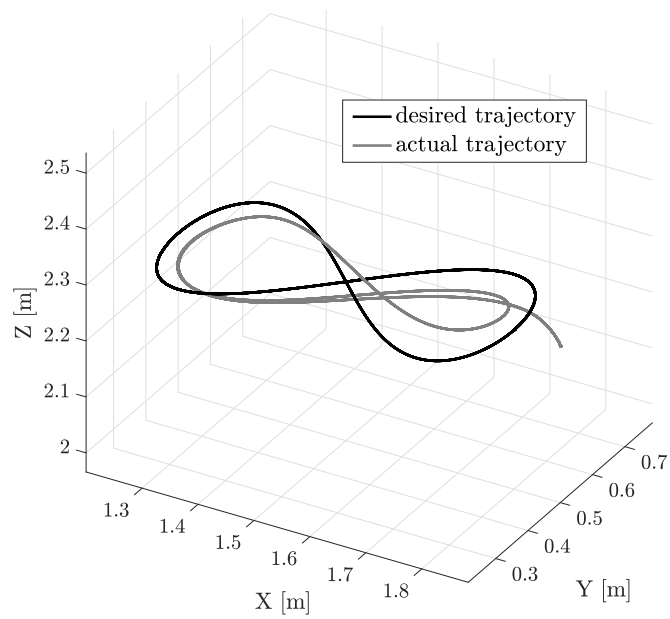
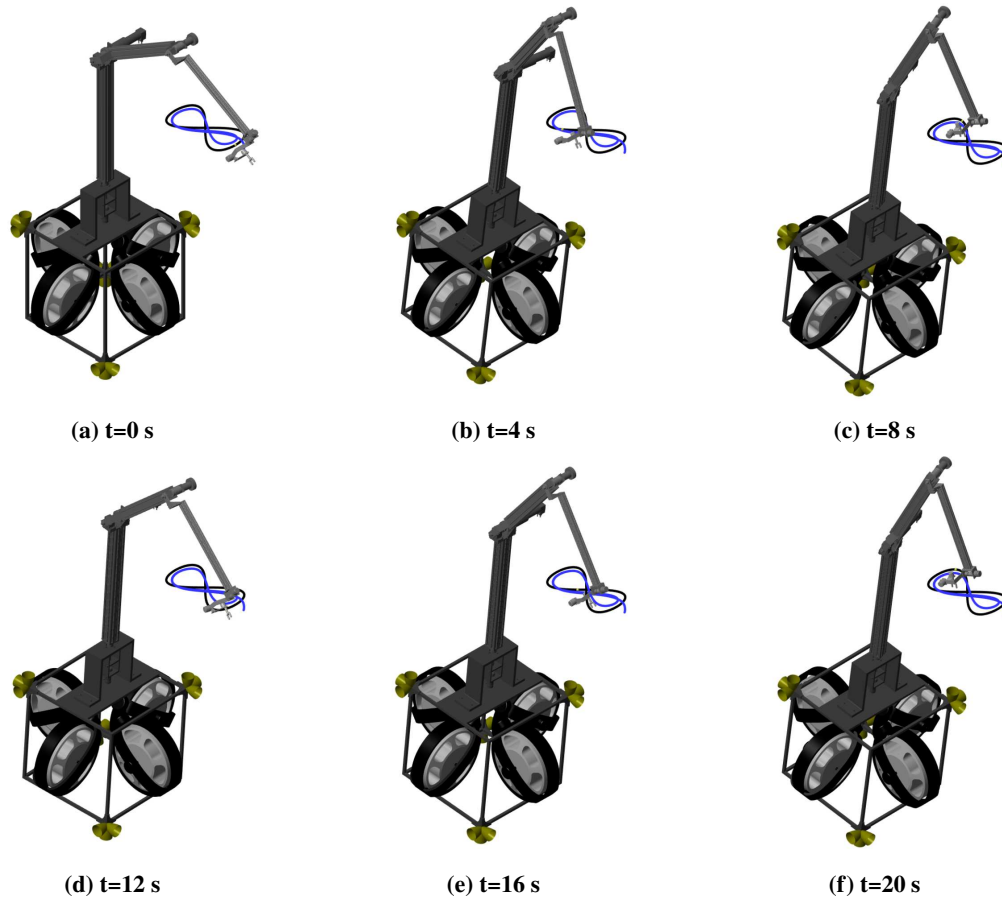


(b) Base attitude and position



(c) Position and velocity tracking errors

Fig. 5 Lemniscate trajectory tracking performance, non-controlled base.



(g) Desired and actual trajectory

Fig. 6 Uncontrolled Lemniscate maneuver. Screenshot of the simulator outputs. The complete animation can be found at https://youtu.be/tg_nHvPuY1g.

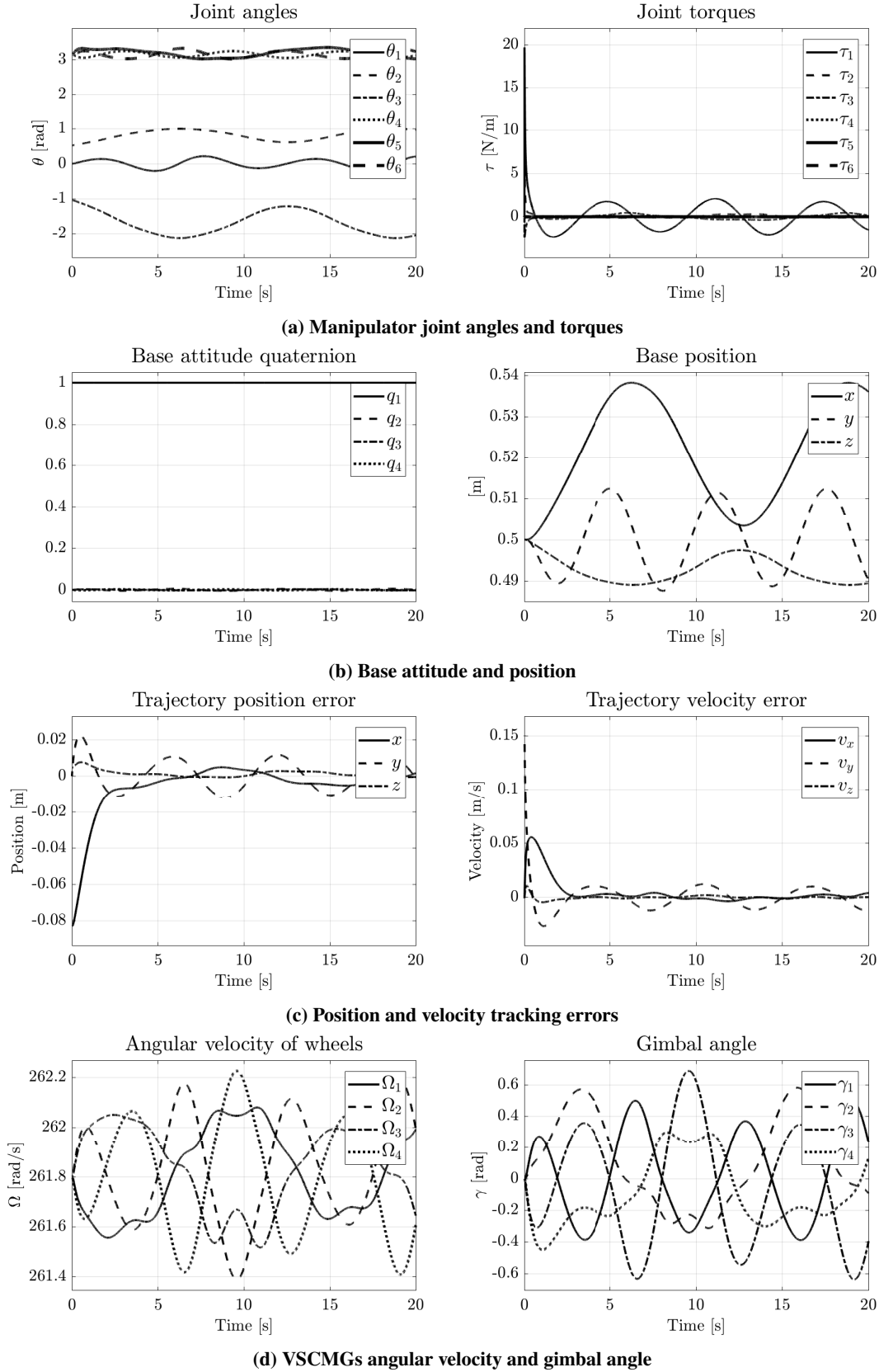
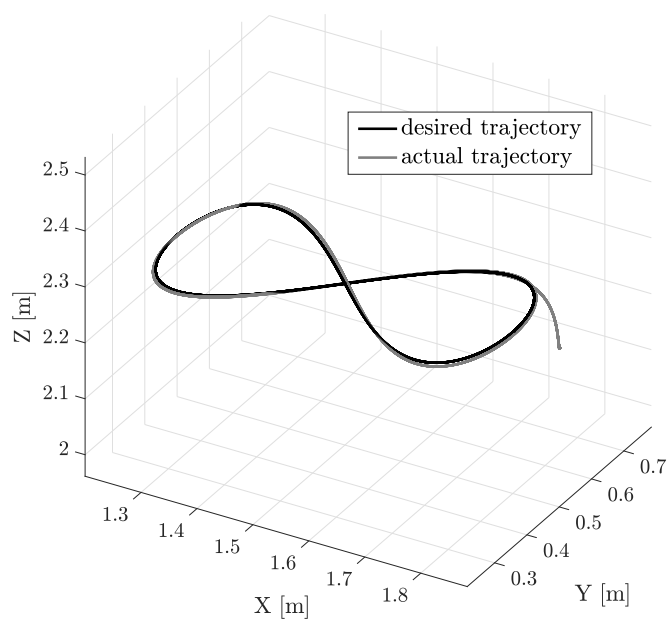
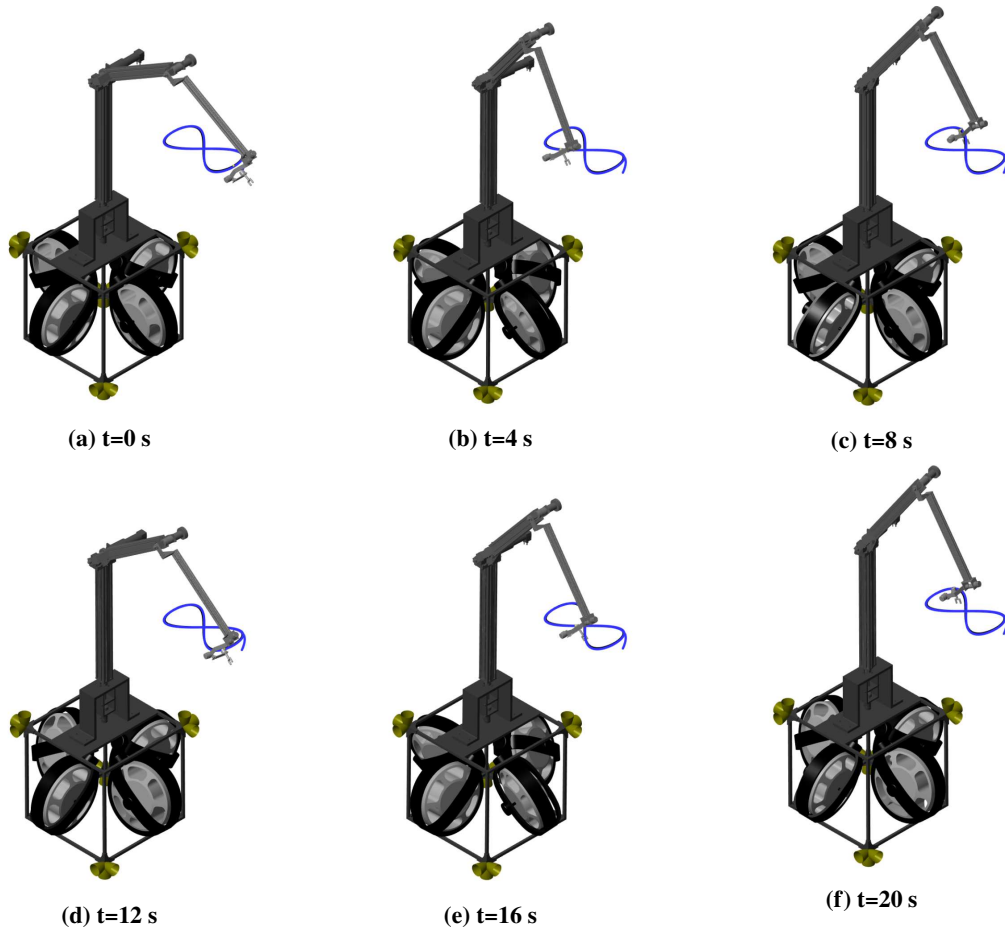
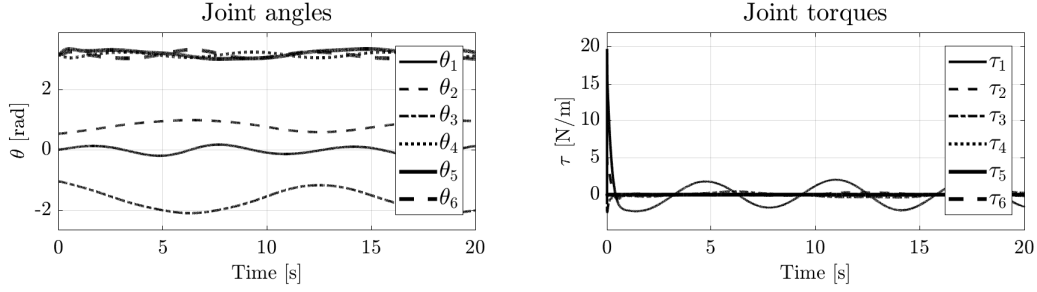


Fig. 7 Lemniscate trajectory tracking performance, VSCMGs controlled base.

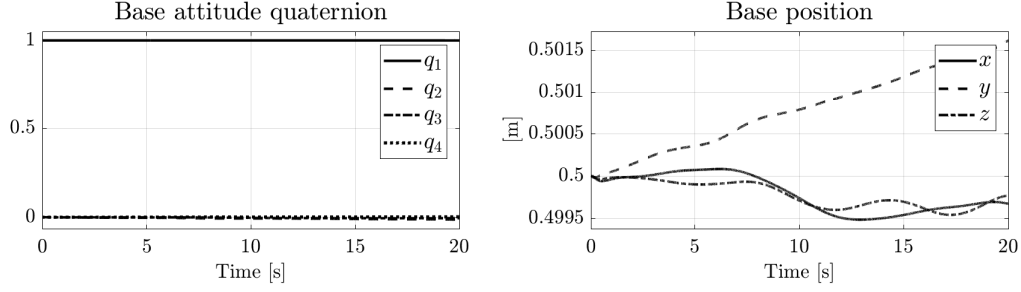


(g) Desired and actual trajectory

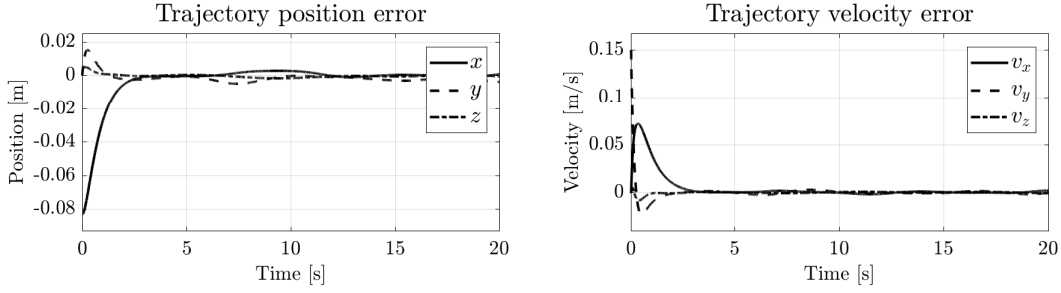
Fig. 8 VSCMGs controlled Lemniscate maneuver. Screenshot of the simulator outputs. The complete animation can be found at <https://youtu.be/sm574qhiscA>. 25



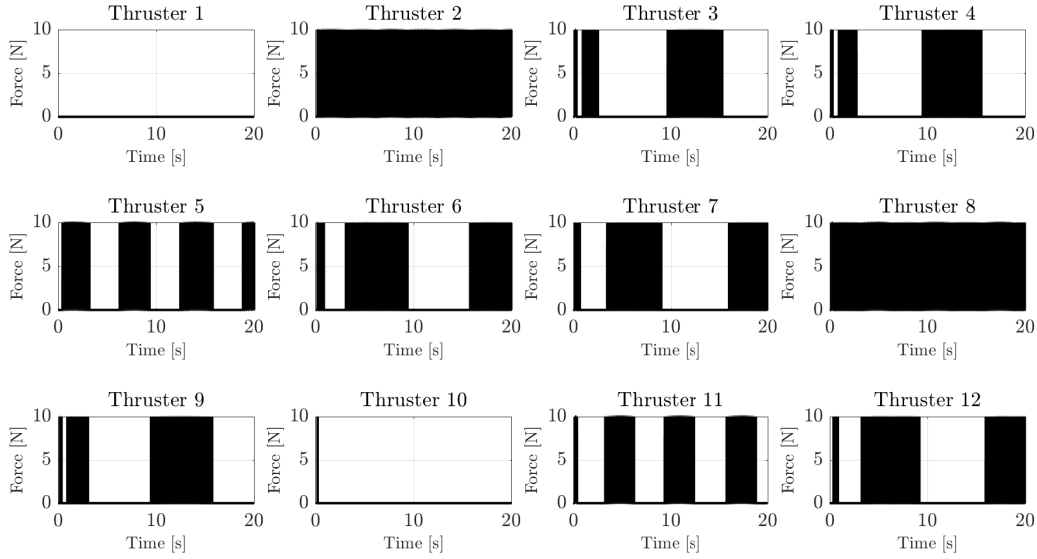
(a) Manipulator joint angles and torques



(b) Base attitude and position

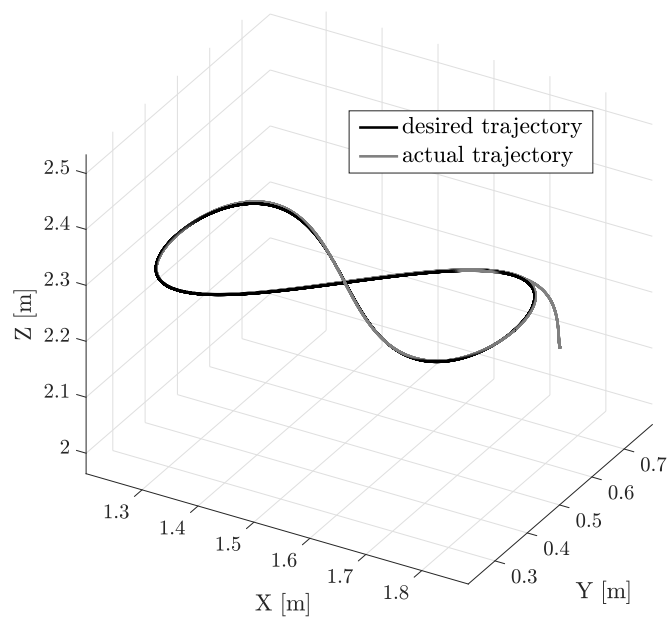
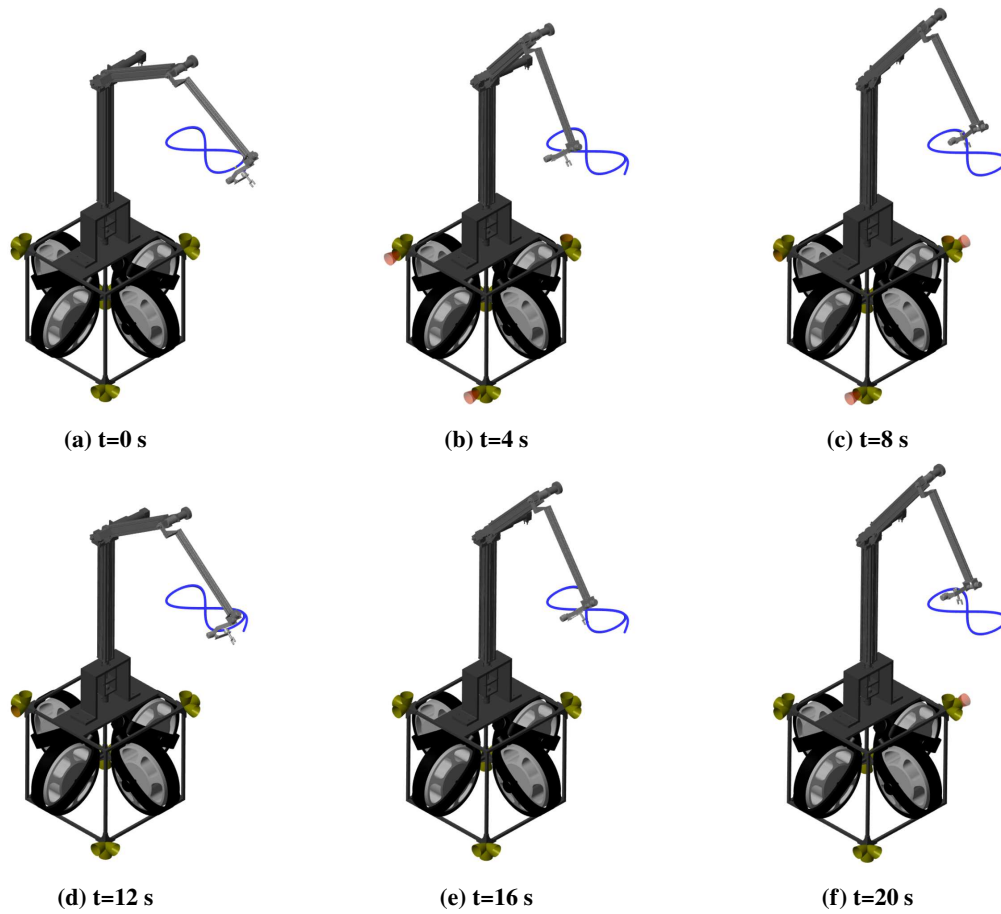


(c) Position and velocity tracking errors



(d) Thrusters Pulse Width Modulation (PWM) firing sequence

Fig. 9 Lemniscate trajectory tracking performance, thruster controlled base.



(g) Desired and actual trajectory

Fig. 10 Thruster controlled Lemniscate maneuver. Screenshot of the simulator outputs. The complete animation can be found at <https://youtu.be/093n3gESqHc>. 27

Appendix A: Simulation Parameters

Table 1 Satellite parameters.

Mass	120 kg
Inertia	$I_{xx} = 12.2 \text{ kg m}^2, I_{yy} = 13 \text{ kg m}^2, I_{zz} = 16.3 \text{ kg m}^2$
Dimensions	$s_x = s_y = s_z = 0.8 \text{ m}$

Table 2 Momentum exchange devices and Thrusters parameters.

Number of VSCMGs	4
Wheel and Gimbal mass	3 kg, 1 kg
Wheel position	$\begin{bmatrix} \pm 0.5 s_x & 0 & 0 \\ 0 & \pm 0.5 s_y & 0 \end{bmatrix}$
I_{ws}	0.042 kg m ²
I_{gs}	0.093 kg m ²
I_{wt}, I_{wg}	0.024 kg m ²
I_{gt}, I_{gg}	0.054 kg m ²
Max gimbal rate	25 deg/s
Max wheel speed	4000 rpm
Max wheel acceleration	700 rpm/s
Maximum thrust	5 N
PWM minimal pulse	15 ms
PWM sampling period	50 ms
PWM resolution	5 ms

Table 3 Manipulator parameters.

LINK'S MASS AND INERTIA					
	Mass	Inertia [I_{xx}, I_{yy}, I_{zz}]			Center of mass
Link 1	16.89 kg	[5.29 4.99 0.32] kg m ²			[0 0 -0.9] m
Link 2	6.59 kg	[0.03 1.89 1.87] kg m ²			[0.394 0 0] m
Link 3	2.71 kg	[0.06 0.78 0.78] kg m ²			[0.413 0 0] m
Link 4	0.59 kg	[$11.5e^{-3}$ $4.07e^{-3}$ $7.54e^{-3}$] kg m ²			[0 0.096 0.049] m
Link 5	0.29 kg	[$1.41e^{-3}$ $1.31e^{-3}$ $1.67e^{-4}$] kg m ²			[0.0045 0.153 0.045] m
Link 6	0.17 kg	[$1.21e^{-3}$ $1.18e^{-3}$ $3.51e^{-5}$] kg m ²			[0 0 0.081] m

DENAVID-HARTENBERG PARAMETERS

	a_i	d_i	α_i	$\theta_{0,i}$
Link 1	0	0	0	0
Link 2	0	0	$\pi/2$	0
Link 3	0.842 m	0	0	0
Link 4	0.849 m	-0.163 m	$-\pi/2$	0
Link 5	0	0	$-\pi/2$	$-\pi/2$
Link 6	0	0	$-\pi/2$	0

References

- [1] Hooker, W. W., "A set of r dynamical attitude equations for an arbitrary n -body satellite having r rotational degrees of freedom," *AIAA Journal*, Vol. 8, No. 7, 1970, pp. 1205–1207. doi:10.2514/6.1969-923.
- [2] Inaba, N., and Oda, M., "Autonomous Satellite Capture by a Space Robot: World First On-orbit Experiment on a Japanese Robot Satellite ETS-VII," *Proceedings of the IEEE International Conference on Robotics and Automation*, Vol. 2, 2000, pp. 1169–1174. doi:10.1109/robot.2000.844757.
- [3] Rodriguez, G., Jain, A., and Kreutz-Delgado, K., "A Spatial Operator Algebra for Manipulator Modeling and Control," *The International Journal of Robotics Research*, Vol. 10, No. 4, 1991, pp. 371–381. doi:10.1177/027836499101000406.
- [4] Jain, A., "Unified Formulation of Dynamics for Serial Rigid Multibody Systems," *Journal of Guidance, Control, and Dynamics*, Vol. 14, No. 3, 1991, pp. 531–542. doi:10.2514/3.20672.
- [5] Featherstone, R., *Rigid Body Dynamics Algorithms*, Springer-Verlag, 2008.
- [6] Jin, J., Park, B., Park, Y., and Tahk, M.-J., "Attitude control of a satellite with redundant thrusters," *Aerospace Science and Technology*, Vol. 10, No. 7, 2006, pp. 644 – 651. doi:10.1016/j.ast.2006.04.005.
- [7] Curti, F., Romano, M., and Bevilacqua, R., "Lyapunov-based thrusters' selection for spacecraft control: analysis and experimentation," *Journal of Guidance, Control, and Dynamics*, Vol. 33, No. 4, 2010, pp. 1143–1160. doi:10.2514/1.47296.
- [8] Jayakody, H. S., Shi, L., Katupitiya, J., and Kinkaid, N., "Robust Adaptive Coordination Controller for a Spacecraft Equipped with a Robotic Manipulator," *Journal of Guidance, Control, and Dynamics*, Vol. 39, No. 12, 2016, pp. 2699–2711. doi:10.2514/1.G002145.
- [9] Walker, M., and Weel, L.-B., "An Adaptive Control Strategy for Space Based Robot Manipulators," *Proceedings of the IEEE International Conference on Robotics and Automation*, Vol. 2, Sacramento, California, United States, 1991, pp. 1673–1680. doi:10.1109/robot.1991.131860.
- [10] Aikenhead, B. A., Daniell, R. G., and Davis, F. M., "Canadarm and the Space Shuttle," *Journal of Vacuum Science & Technology A: Vacuum, Surfaces, and Films*, Vol. 1, No. 2, 1983, pp. 126–132. doi:10.1116/1.572085.
- [11] Xu, Y., Shum, H.-Y., Kanade, T., and Lee, J.-J., "Parameterization and Adaptive Control of Space Robot Systems," *IEEE Transactions on Aerospace and Electronic Systems*, Vol. 30, No. 2, 1994, pp. 435–451. doi:10.1109/7.272266.
- [12] Iwata, T., Kodama, K., Numajiri, F., and Murakami, H., "Experiments on space robot arm path planning using the sensors database," *Journal of Guidance, Control, and Dynamics*, Vol. 22, No. 4, 1999, pp. 573–578. doi:10.2514/2.4419.
- [13] Longman, R. W., Lindbergt, R. E., and Zedd, M. F., "Satellite-mounted robot manipulators—New kinematics and reaction moment compensation," *The International Journal of Robotics Research*, Vol. 6, No. 3, 1987, pp. 87–103. doi:10.1177/027836498700600306.

- [14] Yoshida, K., Kurazume, R., and Y. Umetani, Y., “Dual Arm Coordination in Space Free-flying Robot,” *Proceedings of the IEEE International Conference on Robotics and Automation*, Sacramento, CA, United States, 1991, pp. 2516–2521. doi:10.1109/robot.1991.132004.
- [15] Dubowsky, S., and Papadopoulos, E., “The Kinematics, Dynamics, and Control of Free-flying and Free-floating Space Robotic Systems,” *IEEE Transactions on Robotics and Automation*, Vol. 9, No. 5, 1993, pp. 531–543. doi:10.1109/70.258046.
- [16] Papadopoulos, E., and Dubowsky, S., “Coordinated Manipulator/Spacecraft Motion Control for Space Robotic Systems,” *Proceedings of the IEEE International Conference on Robotics and Automation*, Sacramento, California, United States, 1991, pp. 1696–1701. doi:10.1109/robot.1991.131864.
- [17] Carignan, C. R., and Akin, D. L., “The Reaction Stabilization of On-Orbit Robots,” *IEEE Control Systems Magazine*, Vol. 20, No. 6, 2000, pp. 19–33. doi:10.1109/37.887446.
- [18] Denavit, J., and Hartenberg, R., “A Kinematic Notation for Lower Pair Mechanisms Based on Matrices,” *Transactions of the ASME Journal of Applied Mechanics*, Vol. 22, 1955, pp. 215–221.
- [19] Crassidis, J. L., and Junkins, J. L., *Optimal Estimation of Dynamic Systems*, CRC Press, 2011.
- [20] Luh, J. Y., Walker, M. W., and Paul, R. P., “On-line computational scheme for mechanical manipulators,” *Journal of Dynamic Systems, Measurement, and Control*, Vol. 102, No. 2, 1980, pp. 69–76. doi:10.1115/1.3139629.
- [21] Craig, J. J., *Introduction to Robotics: Mechanics and Control*, 2nd ed., Addison-Wesley Longman Publishing Co., Inc., Boston, MA, USA, 1989.
- [22] Lewis, F. L., Abdallah, C. T., and Dawson, D. M., *Control of Robot Manipulators*, Vol. 236, Macmillan New York, 1993.
- [23] Nenchev, D. N., and Yoshida, K., “Impact analysis and post-impact motion control issues of a free-floating space robot subject to a force impulse,” *IEEE Transactions on Robotics and Automation*, Vol. 15, No. 3, 1999, pp. 548–557. doi:10.1109/70.768186.
- [24] Walker, M. W., and Orin, D. E., “Efficient dynamic computer simulation of robotic mechanisms,” *Journal of Dynamic Systems, Measurement, and Control*, Vol. 104, No. 3, 1982, pp. 205–211. doi:10.1115/1.3139699.
- [25] Nehrenz, M., and Sorgenfrei, M., “A Comparison of Thruster Implementation Strategies for a Deep Space Nanosatellite,” *AIAA Guidance, Navigation, and Control Conference*, 2015, p. 866. doi:10.2514/6.2015-0866.
- [26] Wie, B., *Space Vehicle Dynamics and Control*, AIAA Education Series, American Institute of Aeronautics and Astronautics, 1998.
- [27] Yang, T., “Optimal Thruster Selection with Robust Estimation for Formation Flying Applications,” Ph.D. thesis, Massachusetts Institute of Technology, 2003.
- [28] Yoon, H., and Tsiotras, P., “Spacecraft Adaptive Attitude and Power Tracking with Variable Speed Control Moment Gyroscopes,” *Journal of Guidance, Control, and Dynamics*, Vol. 25, No. 6, 2002, pp. 1081–1090. doi:10.2514/2.4987.

- [29] Spong, M. W., and Vidyasagar, M., *Robot Dynamics and Control*, John Wiley & Sons, 2008.
- [30] Schaub, H., Vadali, S. R., Junkins, J. L., et al., "Feedback control law for variable speed control moment gyros," *Journal of the Astronautical Sciences*, Vol. 46, No. 3, 1998, pp. 307–328. doi:10.2514/1.27351.
- [31] Yoon, H., "Spacecraft Attitude and Power Control Using Variable Speed Control Moment Gyros," Ph.D. thesis, Georgia Institute of Technology, 2004.
- [32] Han, D., Wei, Q., Li, Z., and Sun, W., "Control of Oriented Mechanical systems: A Method Based on Dual Quaternions," *Proceeding of the 17th World Congress, The International Federation of Automatic Control*, International Federation of Automatic Control, Laxenburg, Austria, Seoul, Korea, 2008, pp. 3836–3841. doi:10.3182/20080706-5-KR-1001.00645.
- [33] Filipe, N., and Tsiotras, P., "Rigid Body Motion Tracking Without Linear and Angular Velocity Feedback Using Dual Quaternions," *European Control Conference*, Zürich, Switzerland, 2013, pp. 329–334.
- [34] Wang, X., and Yu, C., "Unit dual quaternion-based feedback linearization tracking problem for attitude and position dynamics," *Systems & Control Letters*, Vol. 62, No. 3, 2013, pp. 225–233. doi:10.1016/j.sysconle.2012.11.019.
- [35] Bryson Jr, A. E., *Control of Spacecraft and Aircraft*, Princeton University Press, 2015.
- [36] Sidi, M. J., *Spacecraft dynamics and control: a practical engineering approach*, Vol. 7, Cambridge University Press, 1997.
- [37] Yoshida, K., "The SpaceDyn: a MATLAB Toolbox for Space and Mobile Robots," *Proceedings of the IEEE/RSJ International Conference on Intelligent Robots and Systems*, Osaka, Japan, 1999, pp. 1633–1638. doi:10.1109/IROS.1999.811712.